

pubs.acs.org/JACS Article

# Iron Heme Enzyme-Catalyzed Cyclopropanations with Diazirines as Carbene Precursors: Computational Explorations of Diazirine Activation and Cyclopropanation Mechanism

Torben Rogge, Qingyang Zhou, Nicholas J. Porter, Frances H. Arnold,\* and K. N. Houk\*



Cite This: J. Am. Chem. Soc. 2024, 146, 2959–2966



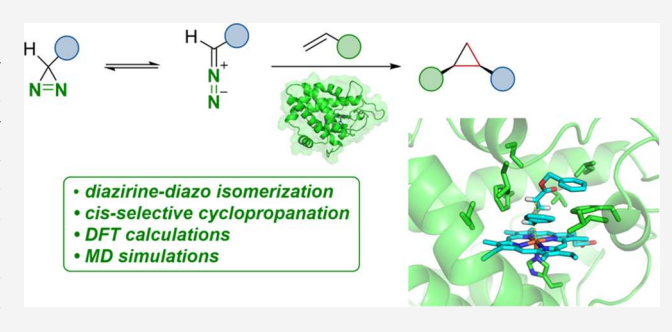
**ACCESS** 

III Metrics & More

Article Recommendations

Supporting Information

ABSTRACT: The mechanism of cyclopropanations with diazirines as air-stable and user-friendly alternatives to commonly employed diazo compounds within iron heme enzyme-catalyzed carbene transfer reactions has been studied by means of density functional theory (DFT) calculations of model systems, quantum mechanics/molecular mechanics (QM/MM) calculations, and molecular dynamics (MD) simulations of the iron carbene and the cyclopropanation transition state in the enzyme active site. The reaction is initiated by a direct diazirine-diazo isomerization occurring in the active site of the enzyme. In contrast, an isomerization mechanism proceeding via the formation of a free

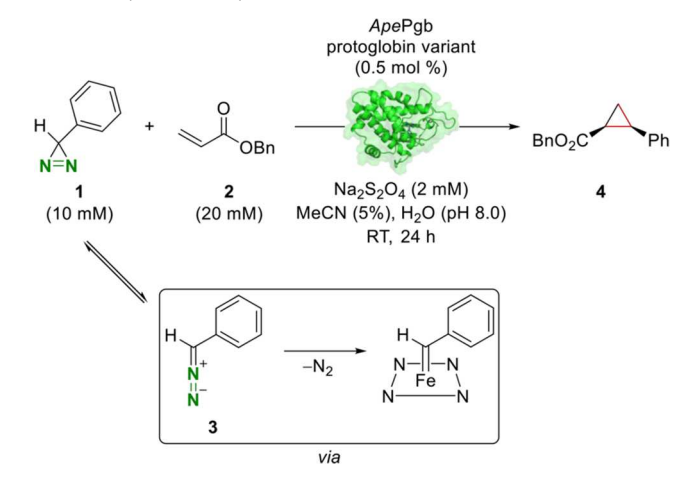


carbene intermediate *in lieu* of a direct, one-step isomerization process was observed for model systems. Subsequent reaction with benzyl acrylate takes place through stepwise C–C bond formation via a diradical intermediate, delivering the cyclopropane product. The origin of the observed diastereo- and enantioselectivity in the enzyme was investigated through MD simulations, which indicate a preferred formation of the *cis*-cyclopropane by steric control.

#### **■ INTRODUCTION**

During the last 2 decades, biocatalysis has attracted expanding attention in academia as well as in the chemical and pharmaceutical industries. In particular, the widespread use of directed evolution has enabled the development of highly efficient and selective enzyme catalysts for a variety of new-tonature transformations, with important applications in, inter alia, molecular synthesis and drug discovery.<sup>2</sup> Bioengineered iron heme enzymes have been shown to facilitate a range of useful non-natural carbene and nitrene transfer reactions.<sup>3</sup> Cyclopropanations and X-H (X = C, N, Si, S, etc.) insertions via iron carbene intermediates were accomplished with iron heme enzyme catalysis, delivering the desired products with outstanding efficiencies and excellent levels of enantioselectivity.4 However, these transformations almost exclusively relied on the use of diazo compounds as carbene precursors, which require the presence of stabilizing electron-withdrawing substituents to avoid potentially hazardous thermal decomposition processes.<sup>5</sup> Recently, bench-stable but challenging-toactivate diazirines have been employed as alternative carbene sources in a variety of carbene transfer reactions, including cisselective cyclopropanations with acrylates (Scheme 1).<sup>6</sup> While experimental mechanistic investigations via trapping experiments provided evidence for a diazirine-diazo isomerization taking place in the presence of the enzyme catalyst and facilitated by the iron heme complex prior to the formation of

Scheme 1. Diazirines for cis-Selective Cyclopropanation with Enzyme Catalysis  $^6$ 



Received: June 8, 2023 Revised: January 4, 2024 Accepted: January 5, 2024

Published: January 25, 2024





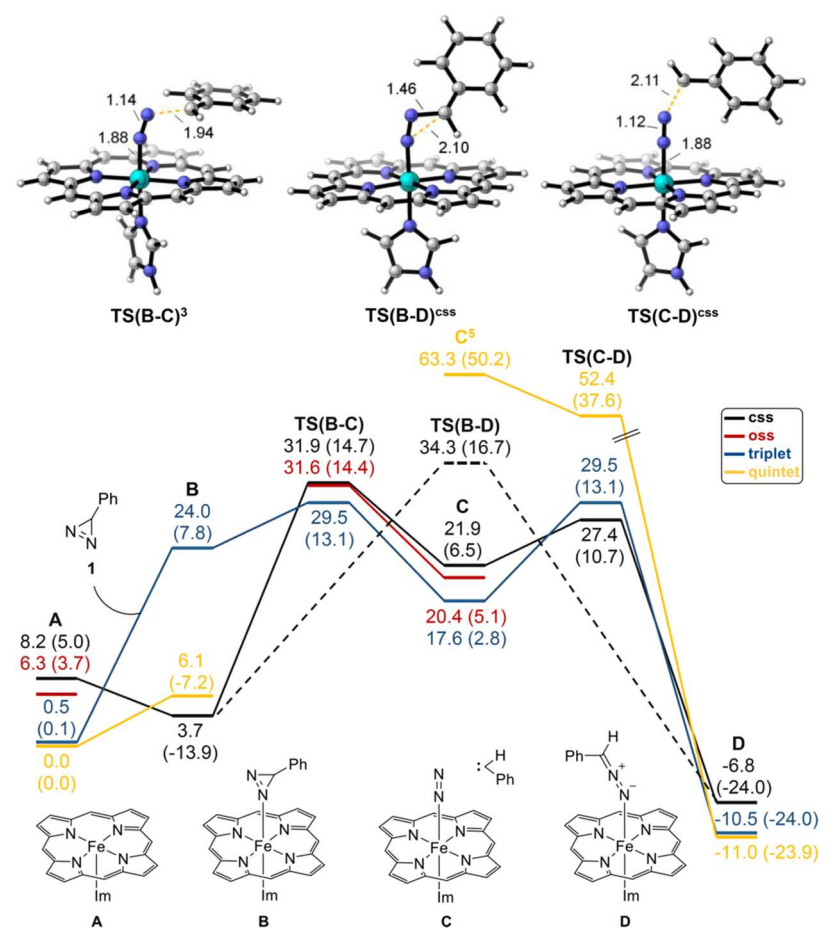


Figure 1. Calculated Gibbs free energy diagram (in kcal  $mol^{-1}$ ) for the isomerization of diazirine 1 to diazo species 3. Values in parentheses correspond to relative enthalpies (in kcal  $mol^{-1}$ ). Distances are given in Å. Superscripts correspond to the spin state. css = closed-shell singlet; oss = open-shell singlet.

the key iron carbene intermediate, a detailed understanding of the complete reaction mechanism is thus far lacking.

We became interested in delineating the mechanism of the diazirine-diazo isomerization as well as the subsequent cyclopropanation reaction by means of density functional theory (DFT) and quantum mechanics/molecular mechanics (QM/MM) calculations. Furthermore, molecular dynamics (MD) simulations in the active site of the enzyme were performed to explore the key iron carbene intermediate as well as the enantio- and diastereoselectivity-controlling factors.

#### RESULTS AND DISCUSSION

We initiated our investigation by studying the formation of phenyldiazomethane (3) via isomerization of 3-phenyl-3*H*-diazirine (1) at the B3LYP-D3(BJ)/def2-TZVP+CPCM-(Et<sub>2</sub>O)//B3LYP-D3(BJ)/6-31G(d),LANL2DZ(Fe) level of theory. In the calculations, an iron(II) porphyrin complex bearing an imidazole ligand in the axial position was employed as a model for the histidine-coordinated iron(II) heme active site in the enzyme, which is formed in the presence of Na<sub>2</sub>S<sub>2</sub>O<sub>4</sub> as reductant. He implicit CPCM solvation model with Et<sub>2</sub>O as the solvent was employed to simulate the hydrophobic environment found inside the active site of the enzyme. Sa,d,e,h In our calculations, a quintet ground state the hydrophobic experimental observations. Starting from the resting state intermediate A, coordination of diazirine 1 via one of the

nitrogen lone pairs results in the formation of intermediate B in a closed-shell singlet (css) spin state via spin-crossover (Figure 1). The subsequent ring-opening of the diazirine motif via transition state TS(B-D) has an activation free energy of 34.3 kcal mol<sup>-1</sup> on the closed-shell singlet surface to lead to intermediate D. The isomerization via TS(B-D) takes place on the css surface and does not represent a stable stationary point in other spin states. However, further investigations revealed an alternative, energetically favorable two-step isomerization process, likely involving a spin-crossover from the closedshell singlet to the triplet spin state. In the first step, carbene intermediate C is formed via TS(B-C) with a Gibbs free energy of activation of 29.5 kcal mol<sup>-1</sup> on the triplet surface and an enthalpic energy barrier of 27.0 kcal mol-1, thus representing the turnover-limiting step. Typically, decreased entropies and enthalpies of activation are observed in the active site of the enzyme, thus resulting in lowered Gibbs free energies of activation. 12 Furthermore, a number of residues surrounding the active site, such as F73, R90, and F93, offer the potential for stabilizing stacking interactions with the phenyl substituent of diazirine 1, thus possibly leading to a further decrease in the Gibbs free energy of activation and allowing for the reaction to occur at room temperature (Figure S10 in the SI). In C, the free carbene remains in relatively close proximity to the coordinated dinitrogen ( $d_{N_2-C} = 3.2$  Å, Figure S4 in the SI) and does not dissociate, thus subsequently allowing for a fast and energetically feasible C-N bond

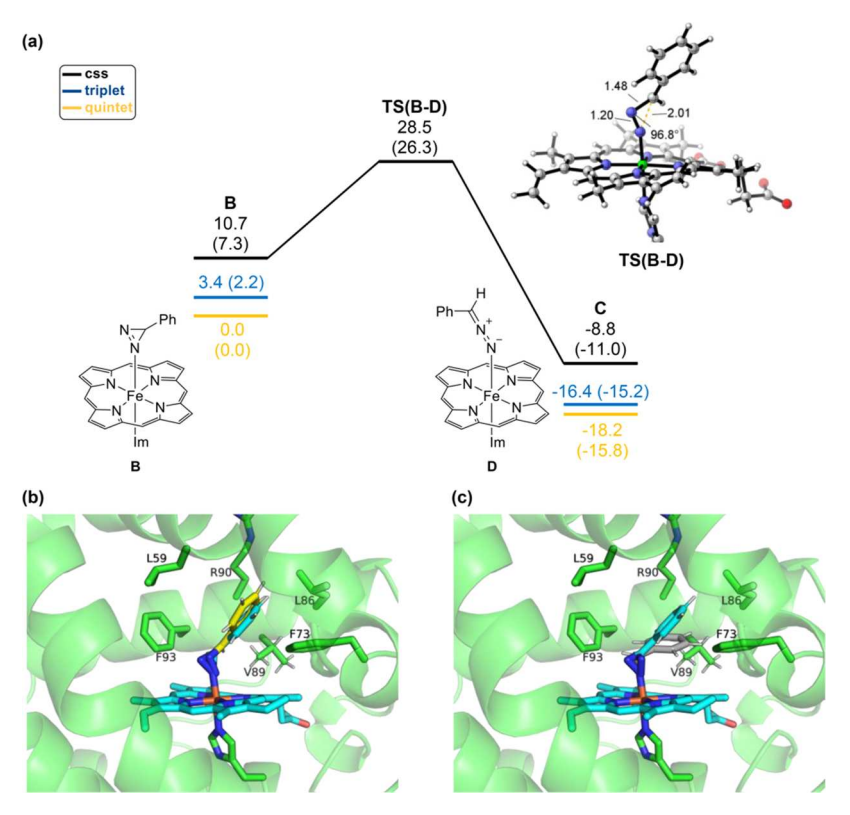


Figure 2. QM/MM calculation of the isomerization step. (a) Calculated Gibbs free energy diagram (in kcal  $mol^{-1}$ ). Values in parentheses correspond to relative enthalpies (in kcal  $mol^{-1}$ ). Distances are given in Å, and peptide residues are omitted for clarity; (b) aligned structure of TS(B-D) (yellow) to  $B^1$  (cyan); (c) aligned structure of DFT-optimized  $B^1$  (gray) to  $B^1$  (cyan). Nonrelevant hydrogens are omitted for clarity in panels (b) and (c).

formation via TS(C-D), resulting in the formation of diazocoordinated complex D and reasonably outcompeting a potential dissociation of phenylcarbene. Presumably, the binding of the diazirine to form complex B in the enzyme is thermally favorable since the higher Gibbs free energy of B with respect to A can be attributed to an unfavorable entropy  $(8-12 \text{ kcal mol}^{-1} - T\Delta S \text{ of a bimolecular reaction})$ . This assumption is further substantiated by the significantly lower relative enthalpies of -13.9 and -7.2 kcal mol<sup>-1</sup> relative to  $A^5$ on the css and quintet spin surface, respectively, thereby highlighting the unfavorable entropy for coordination of diazirine. Furthermore, the substoichiometric concentration of the reductant Na<sub>2</sub>S<sub>2</sub>O<sub>4</sub> renders an involvement of Na<sub>2</sub>S<sub>2</sub>O<sub>4</sub> or a mechanism proceeding via an iron(III) species unlikely for the catalytic diazirine activation. The observation of a two-step mechanism being operative in lieu of a direct diazirine-diazo isomerization pathway is in good agreement with previously reported studies on thermal, metal-free diazirine isomerizations. 13

We also investigated the isomerization process using the QM/MM method, where the whole enzyme is modeled (Figure 2a). In our calculation, substrate, heme, and coordinated histidine are described using DFT, and all of the rest are treated by a MM force field (see the SI for details). Our QM/MM calculations reveal that only the direct isomerization transition state TS(B-D) can be located in the enzyme active site, which means the two-step transition state TS(B-C) and the formation of the corresponding carbene intermediate is disfavored by the enzyme environment (Figures S7 and S8). The barrier from  $B^1$  to TS(B-D) is also lowered dramatically, from 30.6 to 17.8 kcal mol<sup>-1</sup>. In the

structures, we observed  $C-H/\pi$  and  $\pi-\pi$  interactions between the diazirine and surrounding nonpolar side chains (Figure S7). Our computations also reveal that the enzyme preorganizes the conformation of  $B^1$ , causing it to closely resemble the transition state TS(B-D) (Figure 2b). By aligning the DFT-optimized intermediate  $B^1$  in the enzyme site, we found a strong steric repulsion between it and nearby  $\alpha$  helix residues (V89) (Figure 2c). This reveals the enzyme's role in controlling the substrate's binding conformation through the evolution of a structurally rigid scaffold. We believe such substrate prearrangement plays an important role in the catalysis of the enzyme, resulting in the lowering of the barrier and inhibition of formation of the free carbene intermediate.

The mechanism of cis-selective cyclopropanation was investigated next (Figure 3). Initially, intermediate D undergoes a shift in coordination from the terminal nitrogen to the C-N double bond, resulting in the formation of the more stable complex E (Figure S3 in the SI). Subsequently, the key carbene intermediate F is generated by facile C-N bond cleavage via TS(E-F) with an activation free energy of 21.9 kcal mol<sup>-1</sup>. The reaction of **F** with benzyl acrylate (2) takes place in a concerted fashion (TS(F-P)) in a closed-shell singlet spin state, generating the cis-configured cyclopropane P and regenerating initial complex A in a single step. In contrast, on the open-shell singlet and triplet surfaces, a facile, stepwise process involving the formation of diradical intermediate G was observed. Intermediate G is generated by C-C bond formation between the carbene carbon C1 and the terminal alkene carbon  $C_{term}$  in TS(F-G), which is preferred over the concerted cyclopropanation by 2.7 kcal mol<sup>-1</sup>. The observation of a preferred stepwise pathway is further in line with

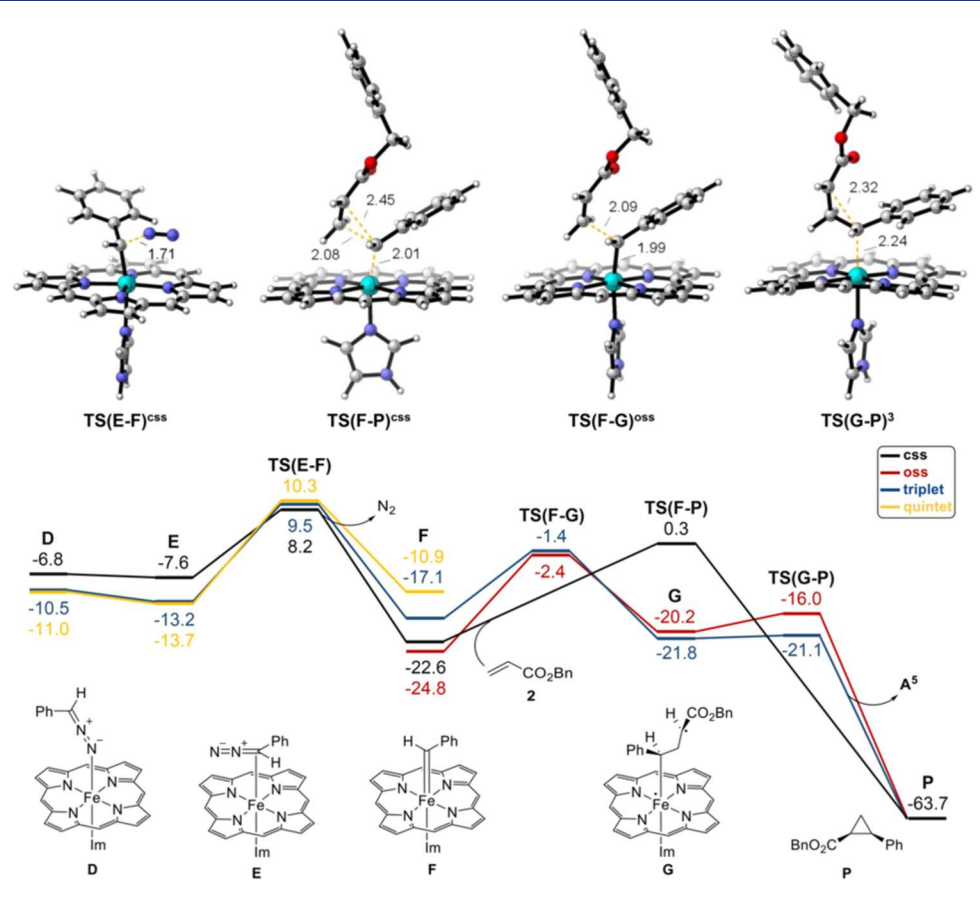


Figure 3. Calculated Gibbs free energy diagram (relative to  $A^5$ , in kcal mol<sup>-1</sup>) for the cyclopropanation with acrylate 2. Distances are given in Å. Superscripts correspond to the spin state. css = closed-shell singlet; oss = open-shell singlet.

previously reported studies on related enzyme-catalyzed reactions. 9b,14 An alternative C–C bond formation taking place with the internal alkene carbon was found to be unfeasible due to significant steric interactions between the ester substituent and the porphyrin ring. Subsequently, the cyclopropane is formed by simultaneous C–C bond formation and Fe–C bond cleavage in **TS(G-P)** with a very low energy barrier of only 0.7 kcal mol<sup>-1</sup>.

In comparison, the formation of the thermodynamically more stable *trans*-configured cyclopropane **P**' occurs via transition state **TS(F-G')** with a 1.9 kcal mol<sup>-1</sup> lower activation free energy than **TS(F-G)** (Figure S2 in the SI). Despite the energetic preference for the generation of the *trans*-cyclopropane, the difference in activation free energy is relatively small, thus enabling the enzyme to preferentially catalyze the formation of the *cis*-configured product by destabilizing one transition state and stabilizing the other.

With the results from the DFT calculations in hand, we turned to molecular dynamics (MD) simulations to gain insights into the structure and dynamics of the active site of the best-performing protoglobin enzyme variant, ApePgb GLAVRSQLL. Employing a monomer of the functional homodimeric enzyme, MD simulations on the carbene intermediate revealed that the side chain of the R63 residue located on a flexible open-loop motif preferentially orients away from the active site and toward the solvent (Figure 4). The preferred orientation of R63 toward the solvent is fully consistent with previously reported cryogenic electron microscopy (cryo-EM) structures of the strongly related enzyme variant ApePgb GLVRSQL, which lacks the additional

V60A, G61V, and F175L mutations present in the fully optimized variant. 6,16 During the directed evolution campaign, the introduction of the V63R, V60A, and G61V mutations into the parent ApePgb enzyme resulted in a considerable increase in cyclopropanation activity, which was attributed to the disruption of a rigid helix region, forming the above-mentioned open loop and thus allowing for easier access to the active site. In addition, a I149L mutation lead to an approximately 2-fold increase in activity, which can be reasonably explained by the further reduced steric congestion in the active site. In contrast, other beneficial mutations, that is, C45G and C102S, are located at distal positions with respect to the active site, while L175 is located directly at the dimer interface and likely influences the activity by modulating the stability of the functional homodimeric enzyme (Figure S9). Furthermore, due to the small size of the carbene, a significant rotation around the Fe-C1 bond was observed in the MD simulations. with the N1-Fe-C1-C2 dihedral fluctuating between 0° and 180° and preferentially adopting a dihedral angle of approximately  $75^{\circ}$  and  $145^{\circ}$ . At a dihedral angle of  $\sim 0^{\circ}$ , a short distance between the phenyl substituent and the F93 side chain was observed, suggesting the presence of stabilizing  $\pi$ – $\pi$ stacking interactions, which were previously observed in cryo-EM measurements of a strongly related carbene intermediate. 16 In contrast, at dihedral angles of 75° and 145°, destabilizing steric interactions between the phenyl substituent and the surrounding hydrophobic residues, in particular, the F73 side chain, are minimized. However, due to the observed large fluctuations and in contrast to the cryo-EM structure, no single preferred conformation is adopted by the carbene,

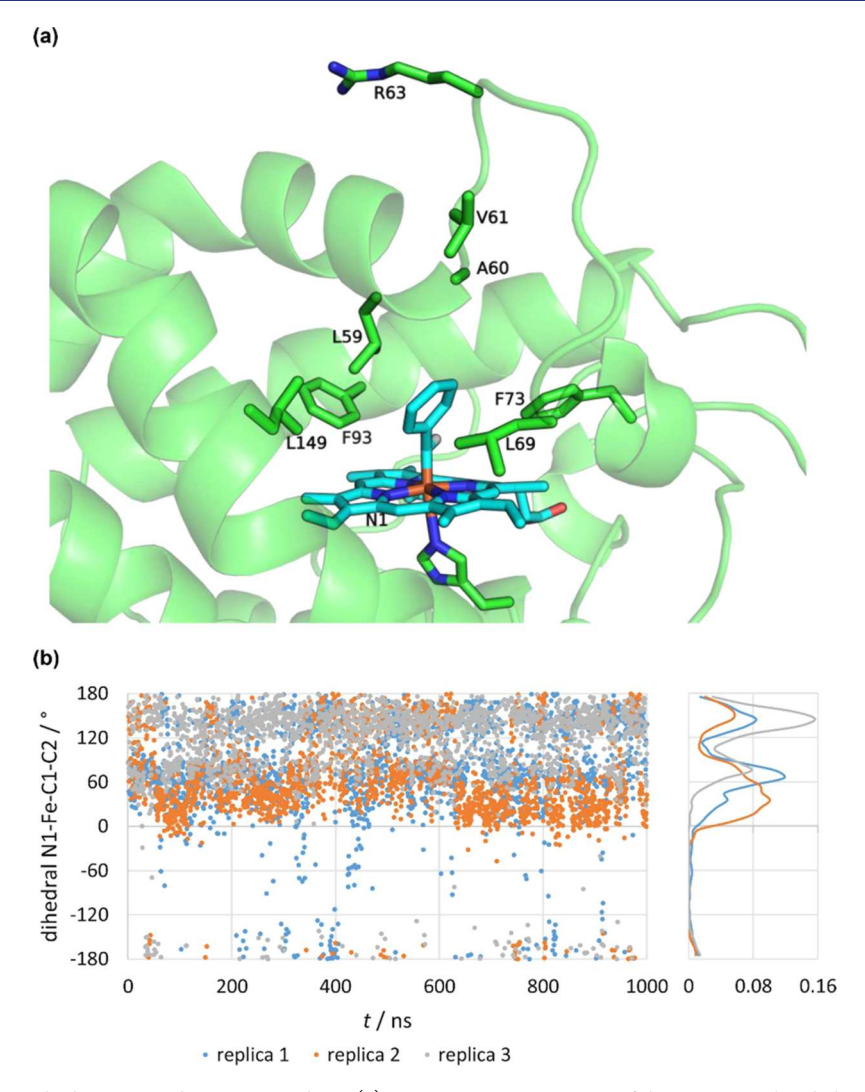


Figure 4. MD simulations on the key iron carbene intermediate. (a) Representative structure of the most populated cluster; (b) plot of the dihedral angle over time (left) and probability density plot (right) for three independent replicas. Nonrelevant hydrogens are omitted for clarity.

thereby indicating that subsequent cyclopropanation can occur from a number of carbene conformations. While a reaction of the carbene with either active site amino acid side chains or the porphyrin can not be fully excluded as a side reaction, it can likely be disregarded due to the hydrophobic nature of all amino acid residues in close proximity.1

To understand the enantioselectivity- and diastereoselectivity-controlling factors in the enzyme, the transition states leading to all four possible isomers were investigated by MD simulations. In the simulations, the Fe-C1, C1-C<sub>term</sub>, and C1-C<sub>int</sub> distances were restrained to mimic the DFToptimized transition state geometries. For the (1S,2R)-isomer, the alkene was found to be preferentially oriented almost perfectly parallel to the Fe-C1 bond, which is in good agreement with the optimal conformation obtained in the DFT calculations (Figure 5a). 18 Furthermore, the benzyl ester substituent is positioned in a sterically accessible area within the active site, thereby minimizing destabilizing interactions. In contrast, the simulations on the TS-like structure leading to the (1R,2S)-configured cyclopropane 4 revealed a significant deviation from the optimal parallel arrangement (Figure 5b). The alkene was found to rotate by approximately 60° to avoid unfavorable steric interactions between the benzyl ester substituent and the large F93, L56, and L59 residues, thus

destabilizing the C-C bond forming transition state and rendering formation of (1R,2S)-4 less feasible.

Structures resulting in the formation of the trans-configured products, i.e., (1R,2R)-4 and (1S,2S)-4, either displayed a significantly broadened distribution of the crucial dihedral angle ranging from 120° to 180° (Figure 5c) or a very unfavorable perpendicular orientation of the alkene with respect to the Fe-C1 bond (Figure 5d), thus rationalizing the experimentally observed high diastereoselectivity.

Based on our simulations, the L56, L59, F73, and F93 residues are crucial for achieving high selectivities in the cyclopropanation reaction. However, the significant steric bulk of these residues likely also prevents efficient cyclopropanations with sterically more demanding olefins from taking place. This observation is in line with a previously reported lack of product formation, when more bulky olefins, i.e., 4-methoxy styrene and allyl benzene, are employed as substrates. Consequently, targeting these sites in future directed evolution campaigns could enable the transformation of a variety of thus far unreactive substrates.

#### **CONCLUSIONS**

In conclusion, we have reported the first detailed investigations on the mechanism of iron heme enzyme-catalyzed cyclo-

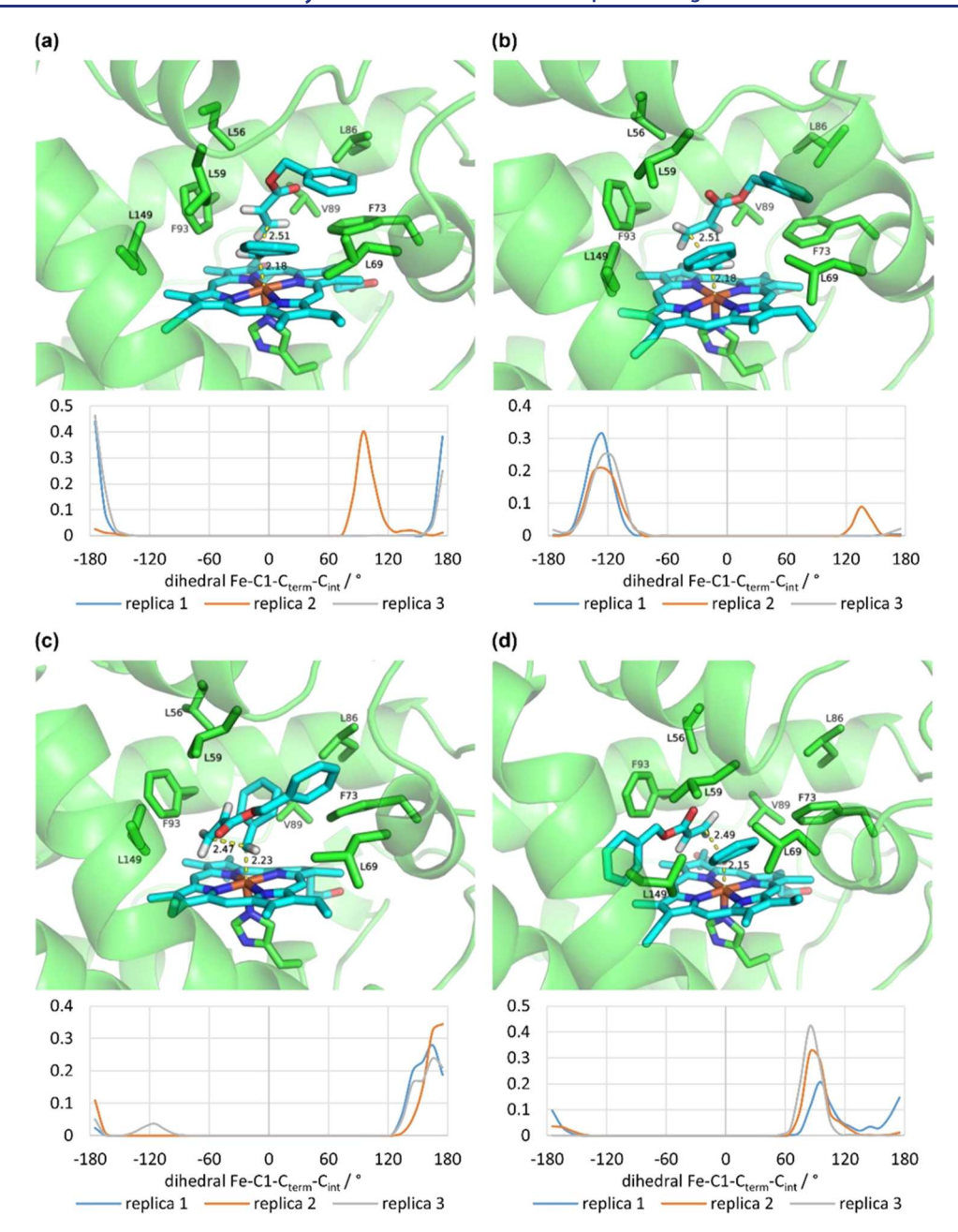


Figure 5. MD simulations on C-C bond forming transition state mimics leading to (a) the major product (1R,2S)-4, (b) (1S,2R)-4, (c) (1R,2R)-4, and (d) (1S,2S)-4. Distances are given in Å. Nonrelevant hydrogens are omitted for clarity.

propanations with stable and user-friendly diazirines as carbene precursors. Our studies revealed a two-step isomerization pathway involving a free carbene intermediate to be operative for structurally simple model systems, while a direct, one-step isomerization mechanism is preferred in the active site of the enzyme. In addition, the cyclopropanation was found to proceed via two energetically feasible distinct C–C bond formations within a diradical mechanism instead of an often proposed concerted process. The origin of diastereo- and enantioselectivity was rationalized through MD simulations of key intermediates and transition state mimics in the enzyme active site.

## ASSOCIATED CONTENT

### Supporting Information

The Supporting Information is available free of charge at https://pubs.acs.org/doi/10.1021/jacs.3c06030.

Computational methods, energies, Cartesian coordinates of calculated structures, and molecular dynamics data (PDF)

# AUTHOR INFORMATION

# **Corresponding Authors**

Frances H. Arnold — Division of Chemistry and Chemical Engineering, Division of Biology and Bioengineering, California Institute of Technology, Pasadena, California 91125, United States; Orcid.org/0000-0002-4027-364X; Email: frances@cheme.caltech.edu

K. N. Houk — Department of Chemistry and Biochemistry, University of California, Los Angeles, California 90095-1569, United States; orcid.org/0000-0002-8387-5261; Email: houk@chem.ucla.edu

#### **Authors**

Torben Rogge — Department of Chemistry and Biochemistry, University of California, Los Angeles, California 90095-1569, United States; Present Address: Technische Universität Berlin, Institute of Chemistry, Straße des 17. Juni 115, 10623 Berlin, Germany; © orcid.org/0000-0002-4519-4596

Qingyang Zhou — Department of Chemistry and Biochemistry, University of California, Los Angeles, California 90095-1569, United States

Nicholas J. Porter — Division of Chemistry and Chemical Engineering, Division of Biology and Bioengineering, California Institute of Technology, Pasadena, California 91125, United States; Present Address: Codexis, Inc., 200 Penobscot Drive, Redwood City, California 94063, United States.

Complete contact information is available at: https://pubs.acs.org/10.1021/jacs.3c06030

#### **Author Contributions**

The manuscript was written through contributions of all authors. All authors have given approval to the final version of the manuscript.

#### **Funding**

This work was supported by the National Science Foundation (CHE-2153972 to K.N.H.), the Alexander von Humboldt-Foundation (Feodor Lynen Fellowship, T.R.), and Merck and the Helen Hay Whitney Foundation (Merck-HHWF Post-doctoral Fellowship, N.J.P.). This publication is based on work supported by the United States Army Research Office under Contract W911NF-19-0026 for the Institute for Collaborative Biotechnologies and the G. Harold and Leila Y. Mathers Charitable Foundation.

#### Notes

The authors declare no competing financial interest.

# ACKNOWLEDGMENTS

Generous support by the National Science Foundation (CHE-2153972 to K.N.H.), the Alexander von Humboldt-Foundation (Feodor Lynen Fellowship, T.R.), and Merck and the Helen Hay Whitney Foundation (Merck-HHWF Postdoctoral Fellowship, N.J.P.) is gratefully acknowledged. Calculations were performed on the Hoffman2 cluster at the University of California, Los Angeles, and Expanse at the San Diego Supercomputer Center (SDSC).

#### REFERENCES

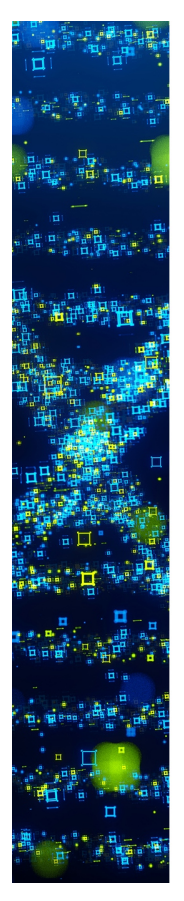
(1) (a) González-Granda, S.; Escot, L.; Lavandera, I.; Gotor-Fernández, V. Chemoenzymatic Cascades Combining Biocatalysis and Transition Metal Catalysis for Asymmetric Synthesis. *Angew. Chem., Int. Ed.* **2023**, *62*, No. e202217713. (b) Zetzsche, L. E.; Chakrabarty, S.; Narayan, A. R. H. The Transformative Power of Biocatalysis in Convergent Synthesis. *J. Am. Chem. Soc.* **2022**, *144*, 5214–5225. (c) Hanefeld, U.; Hollmann, F.; Paul, C. E. Biocatalysis making waves in organic chemistry. *Chem. Soc. Rev.* **2022**, *51*, 594–627. (d) Wu, S.; Snajdrova, R.; Moore, J. C.; Baldenius, K.; Bornscheuer, U. T. Biocatalysis: Enzymatic Synthesis for Industrial Applications. *Angew. Chem., Int. Ed.* **2021**, *60*, 88–119. (e) Winkler,

- C. K.; Schrittwieser, J. H.; Kroutil, W. Power of Biocatalysis for Organic Synthesis. ACS Cent. Sci. 2021, 7, 55–71. (f) Bell, E. L.; Finnigan, W.; France, S. P.; Green, A. P.; Hayes, M. A.; Hepworth, L. J.; Lovelock, S. L.; Niikura, H.; Osuna, S.; Romero, E.; Ryan, K. S.; Turner, N. J.; Flitsch, S. L. Biocatalysis. Nat. Rev. Methods Primers 2021, 1, 46.
- (2) (a) Reetz, M. Making Enzymes Suitable for Organic Chemistry by Rational Protein Design. ChemBioChem 2022, 23, No. e202200049. (b) Wang, Y.; Xue, P.; Cao, M.; Yu, T.; Lane, S. T.; Zhao, H. Directed Evolution: Methodologies and Applications. Chem. Rev. 2021, 121, 12384–12444. (c) Morrison, M. S.; Podracky, C. J.; Liu, D. R. The developing toolkit of continuous directed evolution. Nat. Chem. Biol. 2020, 16, 610–619. (d) Zeymer, C.; Hilvert, D. Directed Evolution of Protein Catalysts. Annu. Rev. Biochem. 2018, 87, 131–157. (e) Packer, M. S.; Liu, D. R. Methods for the directed evolution of proteins. Nat. Rev. Genet. 2015, 16, 379–394.
- (3) (a) Ren, X.; Fasan, R. Engineered and artificial metalloenzymes for selective C–H functionalization. *Curr. Opin. Green Sustainable Chem.* **2021**, 31, No. 100494. (b) Yang, Y.; Arnold, F. H. Navigating the Unnatural Reaction Space: Directed Evolution of Heme Proteins for Selective Carbene and Nitrene Transfer. *Acc. Chem. Res.* **2021**, *54*, 1209–1225. (c) Arnold, F. H. Directed Evolution: Bringing New Chemistry to Life. *Angew. Chem., Int. Ed.* **2018**, *57*, 4143–4148.
- (4) (a) Pott, M.; Tinzl, M.; Hayashi, T.; Ota, Y.; Dunkelmann, D.; Mittl, P. R. E.; Hilvert, D. Noncanonical Heme Ligands Steer Carbene Transfer Reactivity in an Artificial Metalloenzyme. Angew. Chem., Int. Ed. 2021, 60, 15063-15068. (b) Garcia-Borràs, M.; Kan, S. B. J.; Lewis, R. D.; Tang, A.; Jimenez-Osés, G.; Arnold, F. H.; Houk, K. N. Origin and Control of Chemoselectivity in Cytochrome c Catalyzed Carbene Transfer into Si-H and N-H bonds. J. Am. Chem. Soc. 2021, 143, 7114-7123. (c) Kan, S. B. J.; Huang, X.; Gumulya, Y.; Chen, K.; Arnold, F. H. Genetically programmed chiral organoborane synthesis. Nature 2017, 552, 132-136. (d) Bajaj, P.; Sreenilayam, G.; Tyagi, V.; Fasan, R. Gram-Scale Synthesis of Chiral Cyclopropane-Containing Drugs and Drug Precursors with Engineered Myoglobin Catalysts Featuring Complementary Stereoselectivity. Angew. Chem., Int. Ed. 2016, 55, 16110-16114. (e) Kan, S. B. J.; Lewis, R. D.; Chen, K.; Arnold, F. H. Directed evolution of cytochrome c for carbonsilicon bond formation: Bringing silicon to life. Science 2016, 354, 1048-1051. (f) Gober, J. G.; Rydeen, A. E.; Gibson-O'Grady, E. J.; Leuthaeuser, J. B.; Fetrow, J. S.; Brustad, E. M. Mutating a Highly Conserved Residue in Diverse Cytochrome P450s Facilitates Diastereoselective Olefin Cyclopropanation. ChemBioChem 2016, 17, 394-397. (g) Tyagi, V.; Bonn, R. B.; Fasan, R. Intermolecular carbene S-H insertion catalysed by engineered myoglobin-based catalysts. Chem. Sci. 2015, 6, 2488-2494. (h) Coelho, P. S.; Brustad, E. M.; Kannan, A.; Arnold, F. H. Olefin Cyclopropanation via Carbene Transfer Catalyzed by Engineered Cytochrome P450 Enzymes. Science 2013, 339, 307-310.
- (5) Green, S. P.; Wheelhouse, K. M.; Payne, A. D.; Hallett, J. P.; Miller, P. W.; Bull, J. A. Thermal Stability and Explosive Hazard Assessment of Diazo Compounds and Diazo Transfer Reagents. *Org. Process Res. Dev.* **2020**, *24*, 67–84.
- (6) Porter, N. J.; Danelius, E.; Gonen, T.; Arnold, F. H. Biocatalytic Carbene Transfer Using Diazirines. *J. Am. Chem. Soc.* **2022**, *144*, 8892–8896.
- (7) (a) Becke, A. D. Density-functional thermochemistry. III. The role of exact exchange. *J. Chem. Phys.* **1993**, *98*, 5648–5652. (b) Lee, C.; Yang, W.; Parr, R. G. Development of the Colle-Salvetti correlation-energy formula into a functional of the electron density. *Phys. Rev. B* **1988**, *37*, 785–789. (c) Grimme, S.; Ehrlich, S.; Goerigk, L. Effect of the damping function in dispersion corrected density functional theory. *J. Comput. Chem.* **2011**, *32*, 1456–1465. (d) Grimme, S.; Antony, J.; Ehrlich, S.; Krieg, H. A consistent and accurate ab initio parametrization of density functional dispersion correction (DFT-D) for the 94 elements H-Pu. *J. Chem. Phys.* **2010**, *132*, No. 154104. (e) Weigend, F.; Ahlrichs, R. Balanced basis sets of split valence, triple zeta valence and quadruple zeta valence quality for

H to Rn: Design and assessment of accuracy. *Phys. Chem. Chem. Phys.* **2005**, *7*, 3297–3305. (f) Cossi, M.; Rega, N.; Scalmani, G.; Barone, V. Energies, structures, and electronic properties of molecules in solution with the C-PCM solvation model. *J. Comput. Chem.* **2003**, *24*, 669–681. (g) Hay, P. J.; Wadt, W. R. Ab initio effective core potentials for molecular calculations. Potentials for the transition metal atoms Sc to Hg. *J. Chem. Phys.* **1985**, *82*, 270–283.

- (8) Zhang, Y. Computational Investigations of Heme Carbenes and Heme Carbene Transfer Reactions. *Chem. Eur. J.* **2019**, 25, 13231–13247.
- (9) For related computational studies, see: (a) Schaus, L.; Das, A.; Knight, A. M.; Jimenez-Osés, G.; Houk, K. N.; Garcia-Borràs, M.; Arnold, F. H.; Huang, X. Protoglobin-Catalyzed Formation of cis-Trifluoromethyl-Substituted Cyclopropanes by Carbene Transfer. Angew. Chem., Int. Ed. 2023, 62, No. e202208936. (b) Fasan, R.; Vargas, D. A.; Ren, X.; Sengupta, A.; Zhu, L.; Garcia-Borràs, M.; Houk, K. Biocatalytic Strategy for Construction of sp3-Rich Polycyclic Compounds from Directed Evolution and Computational Modeling; Research Square, 2022, DOI: 10.21203/rs.3.rs-1639676/v1. (c) Casali, E.; Gallo, E.; Toma, L. An In-Depth Computational Study of Alkene Cyclopropanation Catalyzed by Fe(porphyrin)-(OCH3) Complexes. The Environmental Effects on the Energy Barriers. Inorg. Chem. 2020, 59, 11329-11336. (d) Lewis, R. D.; Garcia-Borràs, M.; Chalkley, M. J.; Buller, A. R.; Houk, K. N.; Kan, S. B. J.; Arnold, F. H. Catalytic iron-carbene intermediate revealed in a cytochrome c carbene transferase. Proc. Natl. Acad. Sci. U.S.A. 2018, 115, 7308-7313. (e) Wei, Y.; Tinoco, A.; Steck, V.; Fasan, R.; Zhang, Y. Cyclopropanations via Heme Carbenes: Basic Mechanism and Effects of Carbene Substituent, Protein Axial Ligand, and Porphyrin Substitution. J. Am. Chem. Soc. 2018, 140, 1649-1662. (f) Torrent-Sucarrat, M.; Arrastia, I.; Arrieta, A.; Cossío, F. P. Stereoselectivity, Different Oxidation States, and Multiple Spin States in the Cyclopropanation of Olefins Catalyzed by Fe-Porphyrin Complexes. ACS Catal. 2018, 8, 11140-11153. (g) Su, H.; Ma, G.; Liu, Y. Theoretical Insights into the Mechanism and Stereoselectivity of Olefin Cyclopropanation Catalyzed by Two Engineered Cytochrome P450 Enzymes. Inorg. Chem. 2018, 57, 11738-11745. (h) Sharon, D. A.; Mallick, D.; Wang, B.; Shaik, S. Computation Sheds Insight into Iron Porphyrin Carbenes' Electronic Structure, Formation, and N-H Insertion Reactivity. J. Am. Chem. Soc. 2016, 138, 9597-9610.
- (10) For an evaluation of DFT functional performance for spin state prediction, see: Verma, P.; Varga, Z.; Klein, J. E. M. N.; Cramer, C. J.; Que, L.; Truhlar, D. G. Assessment of electronic structure methods for the determination of the ground spin states of Fe(II), Fe(III) and Fe(IV) complexes. *Phys. Chem. Chem. Phys.* **2017**, *19*, 13049–13069.
- (11) Nakamura, M. Spin States in Iron Porphyrins. In Fundamentals of Porphyrin Chemistry; Wiley, 2022; pp 631–659.
- (12) For a review, see: Åqvist, J.; Kazemi, M.; Isaksen, G. V.; Brandsdal, B. O. Entropy and Enzyme Catalysis. *Acc. Chem. Res.* **2017**, 50, 199–207.
- (13) (a) Zapata, L. A.; López, S.; Ruiz, P.; Quijano, J.; Notario, R. Halodiazirines and halodiazo compounds: a computational study of their thermochemistry and isomerization reaction. *Struct. Chem.* 2017, 28, 597–605. (b) Zhang, Y.; Vyas, S.; Hadad, C. M.; Platz, M. S. An Ab Initio Study of the Ground and Excited State Chemistry of Phenyldiazirine and Phenyldiazomethane. *J. Phys. Chem. A* 2010, 114, 5902–5912. (c) Liu, M. T. H.; Choe, Y.-K.; Kimura, M.; Kobayashi, K.; Nagase, S.; Wakahara, T.; Niino, Y.; Ishitsuka, M. O.; Maeda, Y.; Akasaka, T. Effect of Substituents on the Thermal Decomposition of Diazirines: Experimental and Computational Studies. *J. Org. Chem.* 2003, 68, 7471–7478.
- (14) Carminati, D. M.; Fasan, R. Stereoselective Cyclopropanation of Electron-Deficient Olefins with a Cofactor Redesigned Carbene Transferase Featuring Radical Reactivity. ACS Catal. 2019, 9, 9683—9697
- (15) The structure of *Ape*Pgb GLVRSQL (PDB ID: 7UTE) was used as the starting point for the MD simulations with V60A, G61V and F175L mutations manually introduced. For full details, see the Supporting Information.

- (16) Danelius, E.; Porter, N. J.; Unge, J.; Arnold, F. H.; Gonen, T. MicroED Structure of a Protoglobin Reactive Carbene Intermediate. *J. Am. Chem. Soc.* **2023**, *145*, 7159–7165.
- (17) Renata, H.; Lewis, R. D.; Sweredoski, M. J.; Moradian, A.; Hess, S.; Wang, Z. J.; Arnold, F. H. Identification of Mechanism-Based Inactivation in P450-Catalyzed Cyclopropanation Facilitates Engineering of Improved Enzymes. *J. Am. Chem. Soc.* **2016**, *138*, 12527–12533.
- (18) For the DFT-optimized transition state structures, Fe-C1- $C_{term}$ - $C_{internal}$  dihedral angles of 167° and 164° were measured for TS(F-G)<sup>oss</sup> and TS(F-G')<sup>oss</sup>, respectively.



CAS BIOFINDER DISCOVERY PLATFORM™

# STOP DIGGING THROUGH DATA —START MAKING DISCOVERIES

CAS BioFinder helps you find the right biological insights in seconds

Start your search

